ISSN 1615-9306 · JSSCCJ 49 (2) 2026 · Vol. 49 · No. 2 · February 2026

Journal of SEPARATION SCIENCE

2|2026

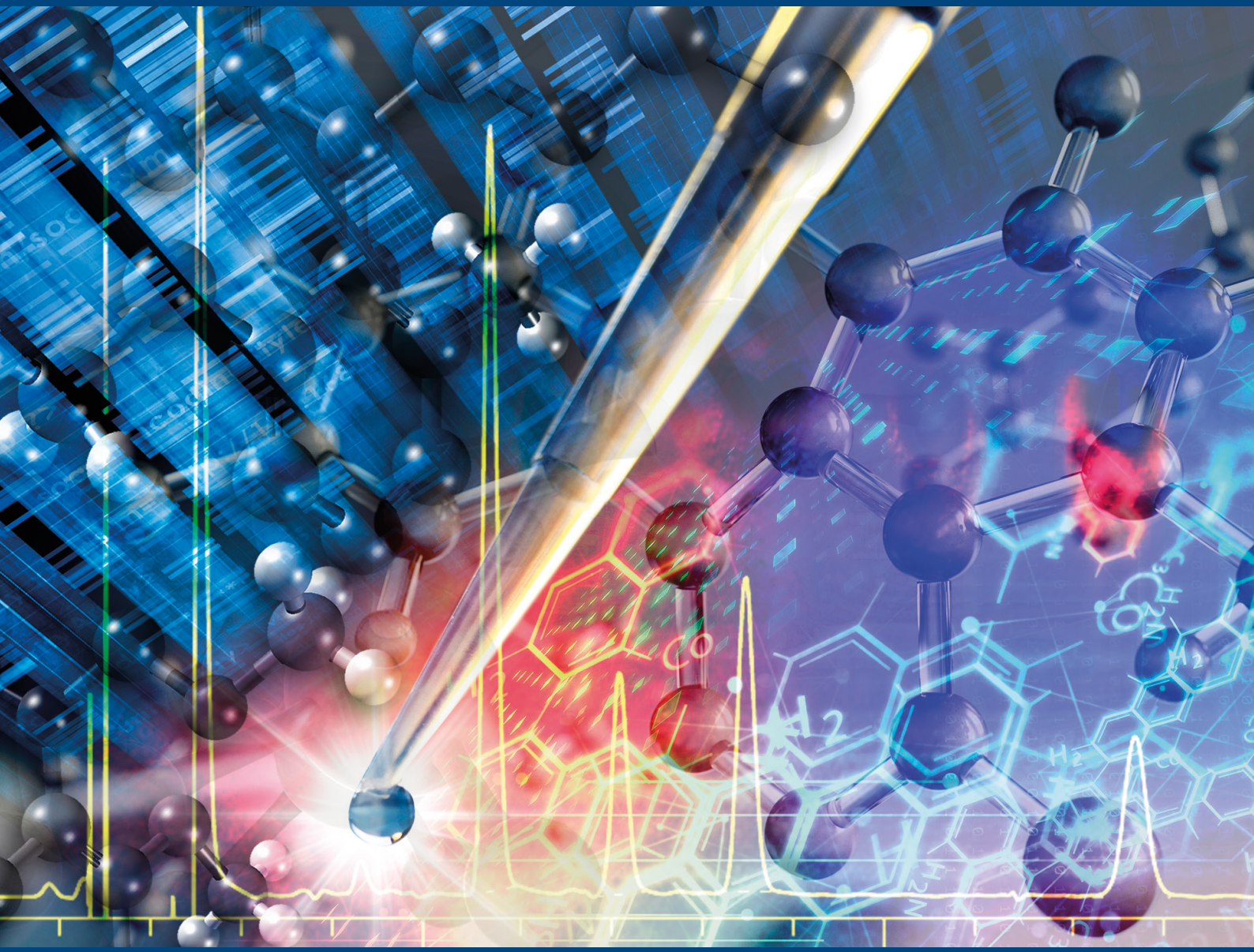

www.jss-journal.com

Methods
Chromatography · Electroseparation

Applications
Biomedicine · Foods · Environment

WILEY VCH

Journal of Separation Science

WILEY-VCH

JOURNAL OF SEPARATION SCIENCE

ORIGINAL ARTICLE

Transposition of the Complementary Developing Solvent Technique to Flash Chromatography: A Structured Step-Based Fractionation Strategy for Complex Plant Extracts

Jason Fauquet[1] | Adam Ellatiff[1] | Claudio Palmieri[1] | Pierre Duez[1] | Bertrand Blankert[2] | Mathilde Wells[2] | Amandine Nachtergael[1]

[1]Laboratory of Therapeutic Chemistry and Pharmacognosy, Research Institute for Health Sciences and Technology, Research Institute for Bioscience, Faculty of Medicine, Pharmacy and Biomedical Sciences, University of Mons (UMONS), Mons, Belgium | [2]Laboratory of Pharmaceutical Analysis, Research Institute for Health Sciences and Technology, Research Institute for Bioscience, Faculty of Medicine, Pharmacy and Biomedical Sciences, University of Mons (UMONS), Mons, Belgium

Correspondence: Jason Fauquet (Jason.FAUQUET@umons.ac.be)

Received: 5 September 2025 | **Revised:** 16 January 2026 | **Accepted:** 27 January 2026

Keywords: HPTLC-to-flash transposition | isocratic step fractionation | preparative chromatography workflow | Universal HPTLC Mix | untargeted metabolomics workflow

ABSTRACT

The Complementary Developing Solvent technique, originally developed for high-performance thin-layer chromatography, employs solvent systems with distinct polarity ranges to achieve enhanced chromatographic resolution while covering a broad chemical space. This study demonstrates the successful adaptation of low polarity developing solvent and high polarity developing solvent systems to normal-phase flash chromatography for systematic fractionation. The system suitability test used in high-performance thin layer chromatography, namely the Universal HPTLC Mix, enabled direct comparisons between high-performance thin layer chromatography and flash chromatography, demonstrating a conserved polarity-driven retention hierarchy across chromatographic scales. To confirm compound identities and elution order, each chromatographic peak was collected and analyzed by tandem mass spectrometry, with MS/MS spectra manually matched against reference standards. Quantitative chromatographic performance was benchmarked using effective peak capacity (Pc), yielding a value of 16.41 for the high-polarity developing system, indicative of a globally balanced separation. In addition, a systematic isocratic step fractionation strategy was implemented by segmenting each elution gradient (low polarity developing solvent and high polarity developing solvent) into seven predefined polarity windows. This strategy was applied on a crude methanolic extract of *Sideritis scardica* Griseb., confirming robust and reproducible fractionation boundaries in a complex botanical matrix. Collecting a single fraction per isocratic step significantly reduces the number of samples for subsequent analysis such as bioassays and untargeted metabolomic profiling, thereby accelerating natural product discovery and dereplication workflows.

1 | Introduction

Chromatographic techniques are essential for the isolation and characterization of bioactive compounds from natural products. While high-performance thin-layer chromatography (HPTLC) remains widely applied for screening purposes, its intrinsic resolution and scalability limitations often require alternative strategies to achieve comprehensive fractionation of chemically complex extracts [1].

The Complementary Solvent Development (CDS) approach was established to address these challenges by combining solvent systems of distinct polarity, namely low- (LPDS), medium- (MPDS), and high-polarity (HPDS) developing solvents [2]. Initially designed for HPTLC applications and optimized for the *African Herbal Pharmacopoeia* [3], CDS adopts an untargeted strategy and has demonstrated efficient separation of diverse chemical classes, including flavonoids, phenolics, and lipids [2, 4]. The performance of CDS under the intrinsic constraints of HPTLC has been documented across multiple studies, highlighting its ability to enhance selectivity and resolution through solvent complementarity [5–7].

Method robustness and reproducibility are central requirements of untargeted chromatographic approaches [8, 9]. In this context, the Universal HPTLC Mix (UHM) was developed as a generic system suitability test (SST), composed of eight reference compounds spanning the full Rf range and enabling standardized quality control across laboratories and experimental conditions [10]. The sensitivity of the UHM pattern to key HPTLC parameters—including relative humidity, plate activity, chamber saturation, solvent composition, and plate quality—has been reported previously [11–13], and predefined Rf acceptance windows are used to support method consistency and inter-laboratory robustness [14]. Unlike targeted SSTs, which assess individual analytes, UHM provides an untargeted evaluation of chromatographic performance across diverse matrices [4, 15].

While CDS and UHM are now well established in HPTLC workflows [2, 3, 10], their transposition to preparative-scale chromatography has remained largely unexplored. In the present study, CDS principles are transposed to normal-phase flash chromatography to establish a systematic and untargeted fractionation framework for complex plant extracts. Rather than implementing all three CDS solvent systems, this work deliberately focuses on a dual-system approach combining HPDS and LPDS to provide orthogonal selectivity across low- and high-polarity constituents while maintaining operational simplicity. The technical rationale for excluding MPDS is detailed in the Section 2. The robustness of this transposition was quantitatively assessed through intermediate precision and peak capacity (Pc) evaluations.

In addition, a structured isocratic step-based fraction collection strategy is introduced, in which fractions are defined by predefined solvent composition steps rather than individual chromatographic peaks. This approach provides a reproducible and sample-independent framework for fraction collection and is intended to support downstream biological or chemical investigations, while avoiding the complexity and variability associated with conventional peak-based collection strategies commonly used in bio-guided fractionation workflows [16].

As a proof of concept, a methanolic extract of *Sideritis scardica* Griseb., was selected due to the high chemical diversity and broad polarity range of its secondary metabolites. The methanolic extract is characterized by a complex phytochemical profile dominated by polyphenols (notably phenylethanoid glycosides and polyhydroxylated flavones) [17, 18]. This specific extract also contains significant amounts of diterpenes, iridoids, and coumarins [19, 20]. Such a chemically complex matrix serves as an ideal model to illustrate the practical implementation of CDS-derived principles and structured step-based fractionation, demonstrating the method's ability to effectively partition diverse metabolite families into standardized windows.

2 | Material and Methods

2.1 | Chemicals and Materials

All the chemicals and consumable materials used in this study are listed in Table S1.

The composition, chemical, and physical properties of the UHM are provided in Table 1.

The preparation and specific ratios of the solvent mixtures are described by Do et al. [2].

All the materials and chemicals were stored under the appropriate conditions recommended by the manufacturer to maintain their stability and integrity throughout the experiments.

2.2 | Plant Material

The plant material used in this study consisted of cultivated *S. scardica* Griseb., was purchased from the herbal shop Botano (Listaros, Crete, Greece). According to the supplier, the specimens were professionally cultivated in Northern Greece. Upon receipt, the plant was ground to a particle size of less than 0.5 mm and subsequently stored at −20°C until extraction.

2.3 | Plant Extraction

The extraction of *S. scardica* Griseb. was performed according to the protocol described by Taco et al. [24], with minor modifications. Briefly, 1.00 g of micronized plant powder (0.5 mm) was placed in a Retsch MM400 mixer mill (Retsch, Germany) with 20.00 g of methanol and five metal beads (1.0–1.5 mm diameter). The mixture was processed at 30 Hz for 10 min, followed by centrifugation at 4000 × *g* for 20 min. The resulting supernatant was collected and evaporated to dryness using a Rotavapor R-215 (Büchi, Switzerland). The dry extract was then reconstituted in methanol at a concentration of 20 mg/mL and aliquoted into 5 mL Eppendorf tubes. The aliquots were concentrated using a miVac vacuum concentrator (40°C, 12 mbar, 120 min; SP Genevac miVac SpeedTrap [SP Genevac, UK]) and subsequently stored at −20°C until further analysis.

TABLE 1 | Composition and mass spectrometry data for UHM based on Schmid et al. [14]. The Log *P* values are either published or computed* and both were obtained from DrugBank, PubChem, or SciFinder [21–23].

Label	Name	Log *P*	M.W (g/mol)	Polarity	Precursor (*m*/*z*)	CE (eV)	MS/MS reference spectrum (Databases)
1	Guanosine	−1.90	283.24	Positive	284	10	Guanosine Mass Spectrum
2	Sulisobenzone	0.88*	308.31	Negative	307	−40	Sulisobenzone Mass Spectrum
3	Thymidine	−0.93	242.23	Negative	241	−20	Thymidine Mass Spectrum
4	Paracetamol	0.46	151.16	Positive	152	20	Acetaminophen Mass Spectrum
5	Phthalimide	1.15	147.13	Negative	146	−35	1H-Isoindole-1,3(2H)-dione Mass Spectrum
6	9-Hydroxyfluorene	2.84*	182.22	Positive	182	45	9H-Fluoren-9-ol
7	Thioxanthen-9-one	3.90*	212.27	Positive	213	50	Thioxanthen-9-one Mass Spectrum
8	Octrizole	5.88*	323.43	Positive	324	40	Octrizole Mass Spectrum

2.4 | HPTLC Analysis

HPTLC analyses were conducted in strict compliance with the European Pharmacopoeia General Chapter 2.8.25 and the USP General Chapter ⟨203⟩ [25, 26], under the conditions described by Do et al. [2]. The chromatographic separations were performed using silica gel 60 F_{254} glass HPTLC plates (20 cm × 10 cm), employing CAMAG HPTLC systems (Muttenz, Switzerland) equipped with an Automatic TLC Sampler (ATS 4), Automatic Developing Chamber (ADC 2), Derivatizer, TLC Visualizer 2, and visionCATS software v 2.5.18072.1 to ensure robust and reproducible analysis.

The mobile phases were prepared as Do et al. [2]: HPDS (ethanol, dichloromethane, water, formic acid 43:43:11:3 [v/v]) and LPDS (toluene, ethyl acetate 9:1 [v/v]). An HPTLC sample, referred as the UHM sample, was prepared in methanol and consisted of a mixture of the eight UHM compounds (Table 1), with each compound individually dissolved at 1 mg/mL in the final mixture. The methanolic extract of *S. scardica* was prepared at a concentration of 20 mg/mL. Reference standards, comprising individual solutions of each UHM compound, were also prepared in methanol at a concentration of 1 mg/mL to facilitate the identification of each spot in the sample. Flash chromatography fractions obtained from the UHM were prepared in methanol at 1 mg/mL, while fractions derived from the *S. scardica* extract were prepared at 2 mg/mL. The application involved 2 µL of the UHM sample, reference standards, and UHM flash fractions. For the *S. scardica* extract and its corresponding flash fractions, 5 µL were applied. All samples were applied at a controlled rate of 100 nL/s, forming 8 mm bands spaced 11.4 mm apart, with an initial track positioned 20 mm from the plate edge. Prior to development, the plates were conditioned to 33% relative humidity via exposure to saturated $MgCl_2$ aqueous solutions for 10 min, thereby stabilizing analyte adsorption. Chromatographic development was executed either with chamber saturation (HPDS, 20 min, including a saturation pad) or without saturation (LPDS), extending to a migration distance of 70 mm, followed by a 5-min drying step to remove residual solvent.

Post-separation visualization for the UHM sample and its corresponding flash fractions was conducted under shortwave UV (254 nm). For the *S. scardica* extract and its flash fractions, plates were derivatized using the Neu/PEG reagent, consisting of diphenylboric acid 2-aminoethyl ester (NP reagent, 1% w/v in methanol) followed by polyethylene glycol 400 (PEG 400, 5% w/v in ethanol), and subsequently visualized under UV at 366 nm.

2.5 | Flash Chromatography Analysis

2.5.1 | Instrumentation and Data Processing

Flash chromatography was performed using two instruments to optimize the analysis time: Interchim PuriFlash 215 (SN: PF215-B-03-UC; Montluçon, France) and Büchi Pure C-850 FlashPrep (SN: 1000335919; Flawil, Switzerland). Data acquisition and visualization were performed using Interchim v5.0 g.19 and Pure v1.7.1000.27882, respectively. Data analyses were conducted using Spyder version 5.5.1. Custom-developed Python 3.13 scripts were used to process, standardize, and visualize the data (see Supporting Information). These scripts relied on the Pandas library for data parsing and cleaning, and the Matplotlib library for the generation of dual-axis chromatograms (signal vs. gradient). The scripts notably enabled the normalization of data to a maximum of 50 column volumes (CV) and the automated mapping of ELSD/UV signals onto the solvent step-gradient. The HPDS method was transposed and optimized using Interchim PuriFlash 215, whereas the LPDS was transposed and optimized using Büchi Pure C-850 FlashPrep. The same reference of column and dryload were used for both instruments.

2.5.2 | Preparation of DryLoad

Two distinct sample types were prepared for flash chromatography: a synthetic mixture, referred to as the UHM sample, comprising eight UHM compounds (Table 1) and a methanolic extract of *S. scardica*. In both instances, the sample—either the UHM stock solution at a concentration of 1 mg/mL or the plant extract—was combined with silica gel in a mass ratio of five times the total analyte mass (5:1 w/w) to ensure uniform adsorption. Subsequently, the solvent was evaporated under reduced pressure using a Rotavapor R-215 (Büchi, Switzerland), facilitating the homogeneous deposition of the analytes onto the silica matrix. The resulting silica-loaded samples were then sieved through a

0.1 mm mesh to ensure sample homogeneity and the repeatability of subsequent analyses. Finally, the powder was packed into DryLoad cartridges (Pure Solid loader, Büchi) between two frits.

2.5.3 | Selection of the Sample Mass Loaded in the DryLoad Cartridge

The mass of the sample to be loaded in DryLoad was adjusted according to the column characteristics (column format and particle size), as well as the distance between spots (ΔRf) of the compounds on the HPTLC plate. In this study, the column was a 25 g silica column with a particle size of 15 µm (see Table S1). As demonstrated in Figure S1, when ΔRf of the compounds is small (ΔRf 0.10–0.19), the distance between peaks (ΔCV) of compounds will be correspondingly small for flash chromatography (ΔCV 0.4–0.8), according to 1. In addition, complex mixtures, such as plant extracts, frequently exhibit HPTLC migration with small ΔRf, and it was hypothesized that the method should be adapted for small ΔCV. Given that UHM HPTLC spots are frequently in close proximity and occasionally overlap, as illustrated by Do et al. [2], and in line with manufacturer instruction [27], we opted for a sample mass of 240 mg (consisting solely of UHM compounds total mass or the dry plant extract) to prevent any overloading phenomena. This 240 mg sample, which equates to 1440 mg of silica-loaded sample, was subsequently loaded into the DryLoad system.

$$\Delta CV = \frac{1}{Rf_a} - \frac{1}{Rf_b} \quad (1)$$

where *a* and *b* are the two spots on the HPTLC plate. Rf denotes the retention factor in HPTLC. Its inverse indicates chromatographic retention, with lower Rf values showing stronger stationary phase interactions. CV represents CV in flash chromatography, while ΔCV estimates elution distance between compounds, allowing HPTLC to flash chromatography conversion.

2.5.4 | Selection of the Gradient for Solvent Systems

The gradient used in flash chromatography was developed based on the proportions of HPDS, MPDS, and LPDS solvent mixtures, taking inspiration from the transfer techniques described in the Interchim manual [28]. A key adaptation in this transposition involves the controlled increase of the more eluting solvent's proportion beyond that used in HPTLC. This optimizes elution efficiency, enhances separation performance, and improves analyte recovery in flash chromatography. Unfortunately, the MPDS system could not be successfully adapted to normal-phase flash chromatography. To evaluate the feasibility of this transposition, the run was intentionally initiated at maximum elution strength using 100% tetrahydrofuran. Despite these conditions, no elution of UHM compounds was observed and all analytes remained strongly retained on the silica stationary phase. The tested gradient conditions and the observed chromatographic behavior are detailed in Table S8. The HPDS solvent mixture employed in the HPTLC system consisted of dichloromethane, ethanol, water, and formic acid in proportions of 43:43:11:3 (v/v). However, the transition to normal-phase flash chromatography required specific adaptations to ensure system compatibility and metabolite stability. First, water was omitted as normal-phase flash chromatography is not compatible with aqueous mobile phases when using silica-based stationary phases; the presence of water can lead to phase deactivation, impaired mass transfer, and poor reproducibility [29, 30]. Second, the 3% (v/v) formic acid used in HPTLC was excluded to prevent potential acid-catalyzed degradation or structural rearrangement of sensitive metabolites during the longer residence time of the flash process [31, 32].

Consequently, adaptation of the HPTLC solvent system was required to ensure both instrumental compatibility and analyte stability. Ethanol was replaced with methanol based on their comparable protic nature and hydrogen-bonding capacity, while methanol offers lower viscosity, reduced backpressure, and lower operational costs [7, 33]. The objective of this adaptation was to preserve the effective polarity characteristics of the original system while ensuring compatibility with flash chromatography.

The optimized gradient (Figure 1, Table S3) was specifically calibrated to compensate for these changes, beginning with 10 CV in 100% dichloromethane, followed by a gradual increase in the methanol fraction over 20 CV, reaching an isocratic step at 60% methanol.

This 10 CV step at 60% methanol was specifically incorporated to ensure a final elution strength higher than that of the original HPTLC mobile phase, which contained a total of 57% polar and protic modifiers (43% ethanol, 11% water, and 3% formic acid). By reaching 60% methanol—a solvent with higher eluotropic strength than ethanol [7, 34]—this adjustment effectively compensates for the removal of water and acid, guaranteeing the complete recovery of the most polar analytes. The robustness of this adaptation is experimentally supported by the conserved elution order and retention hierarchy of the UHM compounds under HPDS conditions, as illustrated by the direct mapping between HPTLC and flash profiles in Figure 3.

The same logic was applied to the LPDS mobile phase, which, in HPTLC, is composed of toluene and ethyl acetate in a ratio of 90:10 (v/v). The designed gradient (Figure 1, Table S4) was also based on a step gradient. It started with an isocratic step of 10 CV in 100% toluene, followed by a gradual increase in the ethyl acetate content over 20 CV, reaching an isocratic step at 15%. This 10 CV step at 15% ethyl acetate was incorporated to obtain a higher final ethyl acetate concentration than that in HPTLC (15% vs. 10% in HPTLC). The final step of gradient elution was 100% ethyl acetate constituting the rinsing area to ensure complete elution of all eluable compounds. Under both condition (HPDS and LPDS), the flow rate was set at 15 mL/min.

2.5.5 | Structured Isocratic Step-Based Fraction Collection

A structured isocratic step-based fraction collection strategy was implemented to standardize fraction collection during flash chromatography experiments performed using CDS systems. While the design of the HPDS and LPDS step gradients is described in Figure 1, Figure 2 illustrates how these gradients

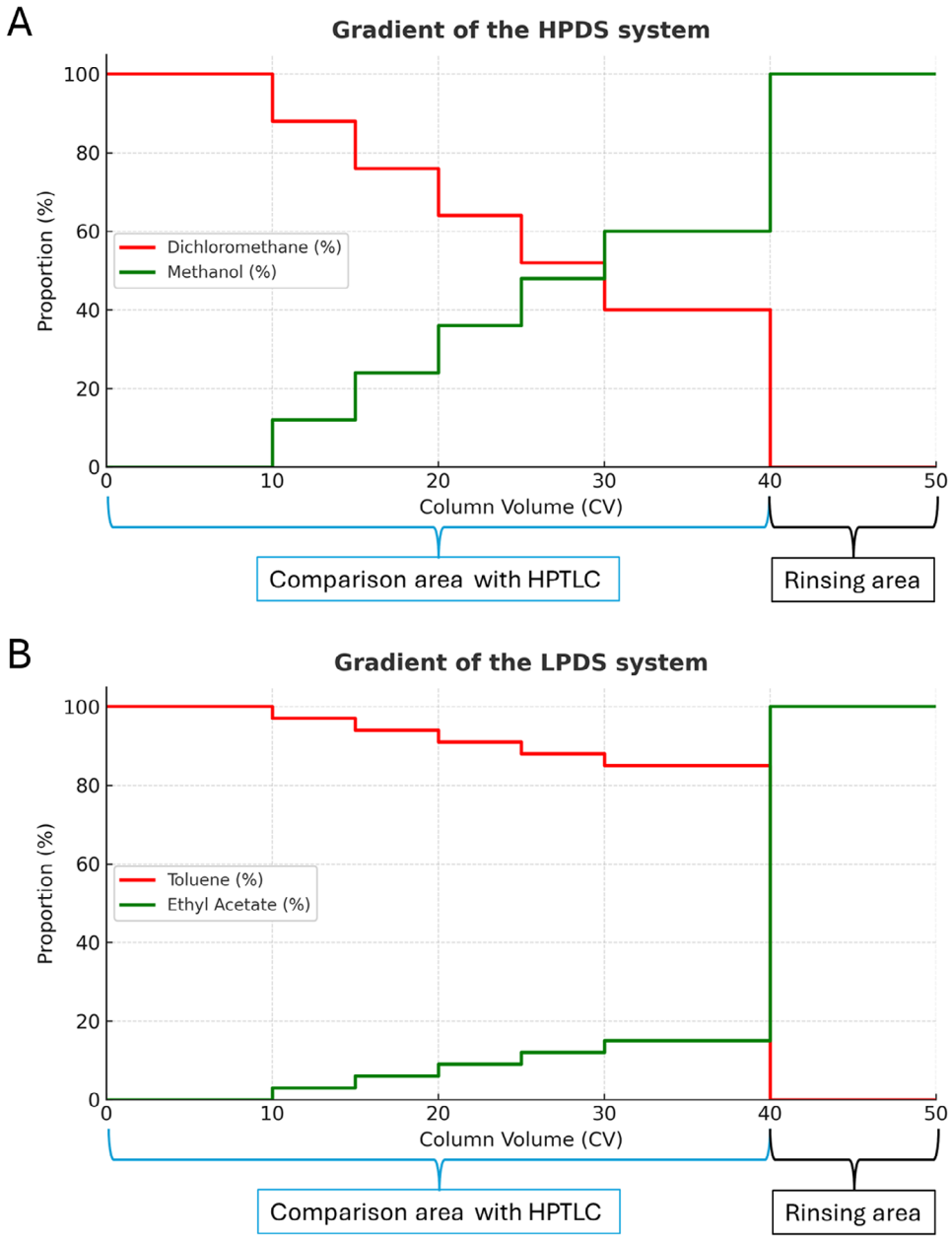

FIGURE 1 | Adapted step gradients for HPDS and LPDS systems in normal-phase flash chromatography. (A) HPDS gradient starting with 10 CV of 100% dichloromethane (red), followed by a stepwise increase in methanol (green) to 60% over 20 CV, a 10 CV isocratic step at 60% methanol, and a final step at 100% methanol. This approach preserves the initial HPDS-like composition while ensuring a higher final methanol proportion than in the corresponding HPTLC system. (B) LPDS gradient starting with 10 CV of 100% toluene (red), followed by a stepwise increase in ethyl acetate (green) to 15% over 20 CV, a 10 CV isocratic step at 15% ethyl acetate, and a final step at 100% ethyl acetate. This approach preserves the initial LPDS-like composition while ensuring a higher final ethyl acetate proportion than in the corresponding HPTLC system.

are operationally translated into a structured isocratic step-based fraction collection scheme.

The strategy relies on the predefined isocratic steps of the CDS solvent systems rather than on individual chromatographic peak detection. For each CDS system applied in this study (HPDS and LPDS), the flash gradient consists of a series of discrete isocratic steps, each corresponding to a fixed solvent composition. Instead of collecting fractions based on peak boundaries, the eluent corresponding to each isocratic step is collected as a single fraction. Consequently, compounds eluting within the same solvent composition window are grouped into a single fraction based on shared polarity characteristics.

In the present configuration, seven isocratic steps were defined per solvent system, resulting in the systematic collection of seven fractions per CDS run, independent of the chromatographic complexity of the injected sample. This fractionation scheme is illustrated in Figure 2, where fractions F1–F7 correspond to successive isocratic steps of the flash gradient. Fraction boundaries are therefore fixed and reproducible and do not depend on sample-specific elution profiles.

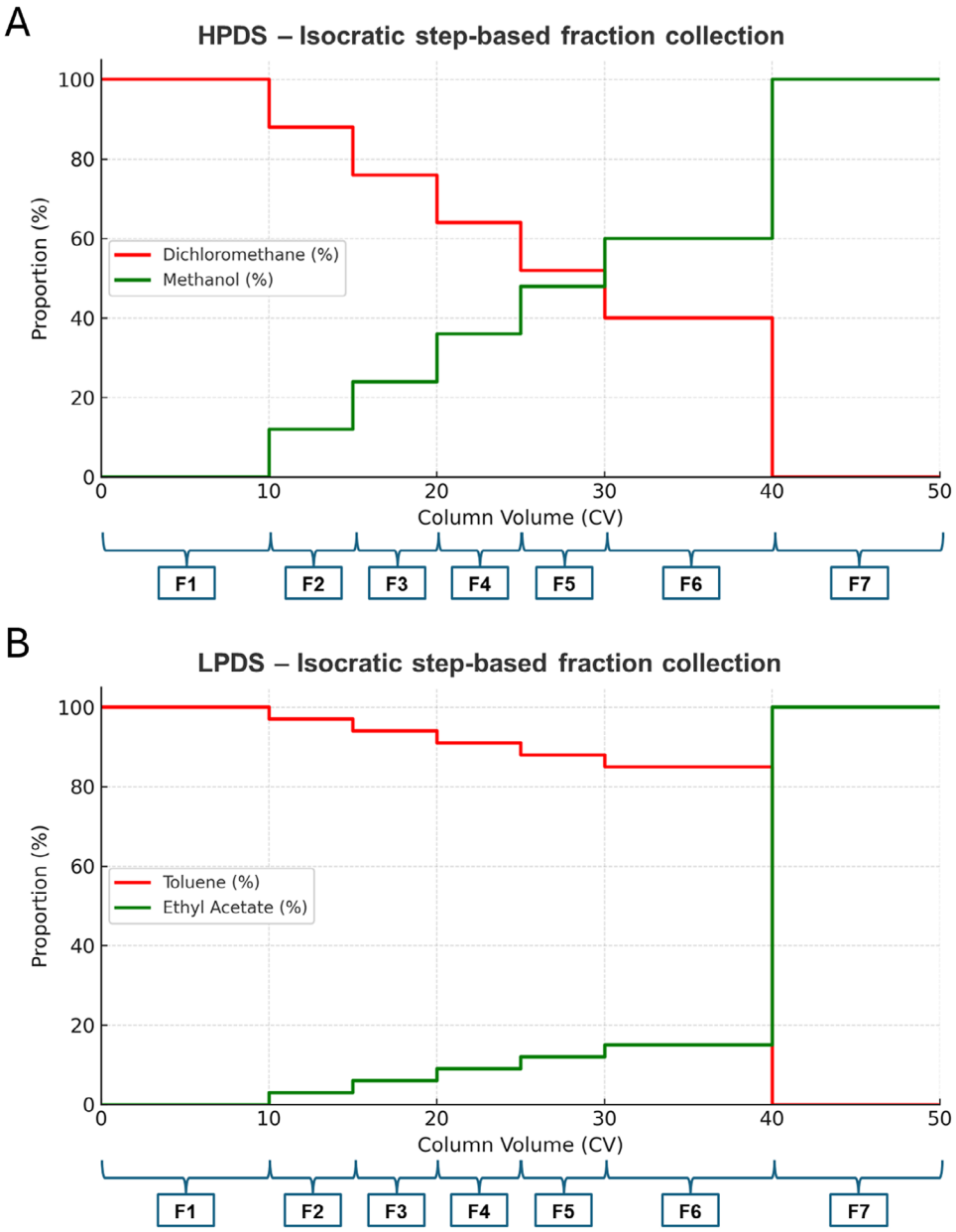

FIGURE 2 | Structured isocratic step-based fraction collection strategy for HPDS and LPDS systems. (A) HPDS system based on dichloromethane (red) and methanol (green). (B) LPDS system based on toluene (red) and ethyl acetate (green). In both cases, the flash gradients are composed of a series of predefined isocratic steps expressed in CV. Each fraction (F1–F7) corresponds to one isocratic step of fixed solvent composition and is collected independently of chromatographic peak detection. Fraction boundaries are therefore fixed and reproducible and do not depend on sample-specific elution profiles.

This step-based fraction collection strategy was not subjected to MS/MS analysis within the scope of the present study.

2.6 | Flash Chromatography of the UHM

2.6.1 | Peak-Based Fraction Collection of the UHM

To substantiate the correlation between HPTLC migration and flash chromatographic elution sequence, peak-based fraction collection was conducted utilizing the UHM. Under both HPDS and LPDS systems, individual chromatographic peaks were isolated based on ultraviolet (UV) and evaporative light scattering detector (ELSD) responses, facilitating the direct assignment of each flash elution position to a specific UHM compound. This peak-based collection was exclusively applied to the UHM and was solely intended to verify the consistency of elution order between HPTLC and flash chromatography, as illustrated in Figures 3 and 4.

2.6.2 | Treatment of UHM Collected Peaks Prior to MS and MS/MS Analysis

Following the individual collection of each peak, the solvent was completely removed under reduced pressure utilizing a

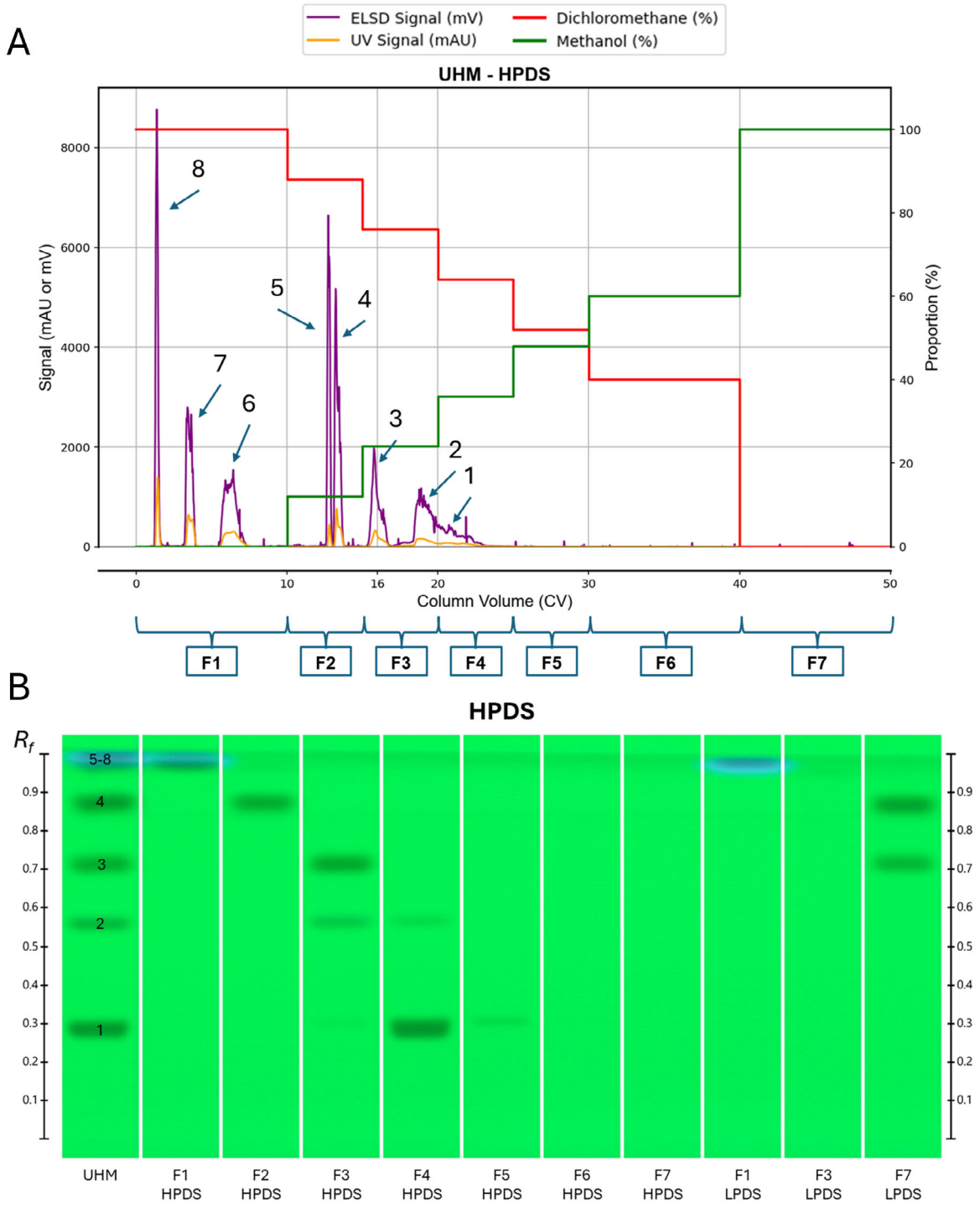

FIGURE 3 | Comparative analysis of flash chromatography and HPTLC separation of the UHM under HPDS conditions. (A) Flash chromatogram obtained using the adapted HPDS solvent system in normal-phase flash chromatography, plotted as a function of CV. The ELSD signal (purple) and UV signal (orange) are overlaid with the stepwise solvent gradient expressed as proportions of dichloromethane (red) and methanol (green). λ (UV): 250–600 nm. Arrows indicate the elution positions of the UHM reference compounds, numbered from the least retained (8) to the most retained (1). The predefined isocratic steps corresponding to the structured flash fractions F1–F7 collected under HPDS conditions are indicated below the chromatogram. A tick mark at 16 CV highlights the boundary corresponding to the LPDS fractionation window. (B) HPTLC plate developed using the HPDS solvent system. Lanes include the UHM reference mixture, HPDS flash fractions F1–F7, and selected flash fractions obtained under LPDS conditions (F1 LPDS, F3 LPDS, and F7 LPDS). Spots are numbered according to increasing polarity, from Compound 8 (least retained) to Compound 1 (most retained). Plate was visualized at 254 nm. This panel enables direct visual comparison between HPDS-derived fractions and selected LPDS-derived fractions on the same HPTLC system, illustrating the relationship and partial overlap between HPDS and LPDS fractionation domains.

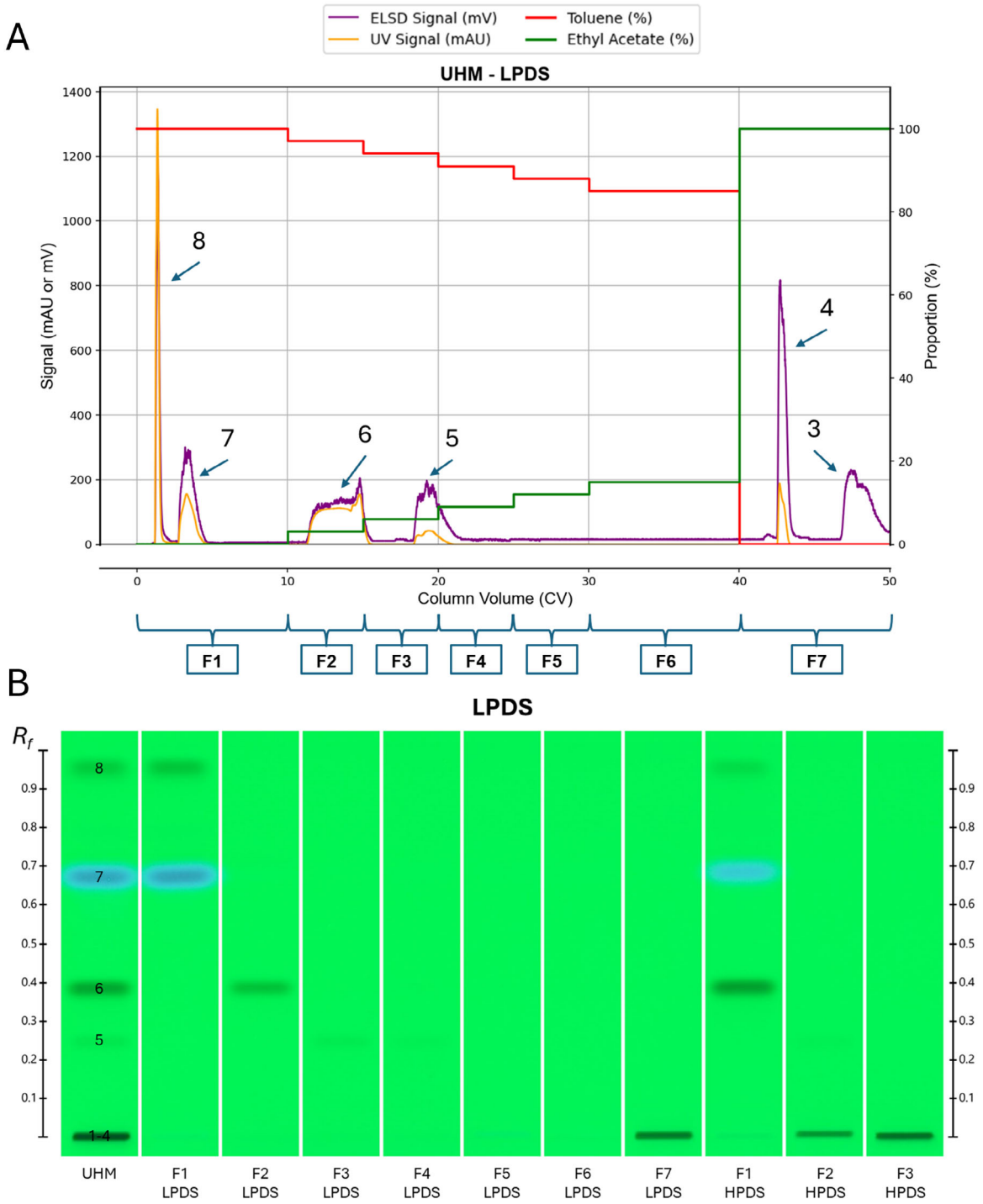

FIGURE 4 | Comparative analysis of flash chromatography and HPTLC separation of the UHM under LPDS conditions. (A) Flash chromatogram obtained using the adapted LPDS solvent system in normal-phase flash chromatography, plotted as a function of CV. The ELSD signal (purple) and UV signal (orange) are superimposed with the stepwise solvent gradient expressed as proportions of toluene (red) and ethyl acetate (green). λ (UV): 290–800 nm. Arrows indicate the elution positions of UHM reference compounds detected under LPDS conditions, numbered from the least retained (8) to the most retained compound observed within the low-polarity region. The predefined isocratic steps corresponding to fractions F1–F7 collected under LPDS conditions are indicated below the chromatogram. (B) HPTLC plate developed using the LPDS solvent system. Lanes include the UHM reference mixture, LPDS flash fractions F1–F7, and selected flash fractions obtained under HPDS conditions (F1 HPDS, F2 HPDS, and F3 HPDS). Spots are numbered according to increasing polarity. Plate was visualized at 254 nm. This panel allows direct visualization of the chemical space covered by LPDS fractions relative to HPDS-derived fractions and highlights the correspondence between both fractionation strategies within the low-polarity domain.

Rotavapor R-215 (Büchi, Switzerland) and subsequently stored at −20°C. Then, each residue was dissolved in methanol LC-MS grade at a concentration of 10 µg/mL prior to MS and MS/MS injection.

2.6.3 | MS and MS/MS Analysis of UHM Sample and Reference Compounds

An AB SCIEX QTRAP 6500+ (SN: DY260232108; Framingham, USA) mass spectrometer was used for all MS and MS/MS analyses. Reference standards, individual solutions of each UHM compounds were prepared in methanol at 10 µg/mL to optimize detection and fragmentation conditions. For reference standards and samples (collected peaks) analysis, full scan mode (MS) was used, followed by product ion scan mode (MS/MS) for targeted fragmentation and identification. Injections were performed via direct infusion at 5 µL/min.

The QTRAP 6500+ mass spectrometer was operated under rigorously controlled conditions to ensure reproducibility of the analytical runs. The source was the Turbo Spray IonDrive. The curtain gas was maintained at 30 psi with an Ion Spray Voltage (IS) of 5000 V for positive polarity (−4500 V for negative polarity) and a source temperature of 50°C. The nebulization conditions included Gas 1 (GS1) at 25 psi and Gas 2 (GS2) at 0 psi to optimize ionization efficiency. For the full scan mode and product ion mode, the compound parameters were compound-dependent and are described in Table S2. In the full-scan mode, spectra were acquired over a mass range of 105–1250 m/z, with a scan rate of 200/s and the Multi-Channel Analysis (MCA) mode disabled. The polarity was compound dependent (Table 1). For the product ion scan mode, the collision gas (CAD) was set to medium, with the collision energy (CE) optimized for each compound, as detailed in Table 1.

Data acquisition and spectral processing were performed using Analyst software v1.7.2. The experimental MS/MS spectra of the reference standards were systematically compared with the validated spectra from MassBank (Table 1) to confirm their molecular identities. For peaks isolated from flash chromatography, MS/MS fragmentation patterns were aligned with the standard spectra to accurately determine the elution order and validate the structural assignments. Representative MS/MS mirror plots for both LPDS and HPDS systems (Compounds 2, 4, 7, and 8) are provided in the Figures S2 and S3 to visually demonstrate the alignment between reference standards and isolated fractions.

2.7 | Quantitative Assessment of Chromatographic Separation

2.7.1 | Intermediate Precision of Chromatographic Retention

The intermediate precision of the chromatographic method was assessed for both HPDS and LPDS solvent systems using the UHM as an SST. Separations were performed in quintuplicate ($n = 5$) over three distinct days by two independent operators.

For each UHM compound, the CV at peak apex (CV_{apex}) was determined from ELSD chromatograms. Mean CV_{apex} values, standard deviations (SD), and relative standard deviations (RSD, %) were calculated to assess the repeatability and robustness of retention behavior across runs, days, and operators. These parameters were used to evaluate the stability of elution order and retention positioning under both solvent systems.

2.7.2 | Peak Base Width Determination

Peak base widths were determined from ELSD chromatograms using a local baseline return criterion. For each chromatographic peak, the mean start (mean CV_{start}) and mean end (mean CV_{end}) positions were defined as the points at which the ELSD signal returned to its local baseline on either side of the apex, thereby avoiding the use of a fixed absolute intensity threshold.

Peak base widths (w) were expressed in CV units and calculated as:

$$w = CV_{end} - CV_{start} \quad (2)$$

The intermediate precision of peak base width determination was evaluated for both HPDS and LPDS systems across independent chromatographic runs. For each UHM compound eluting within the investigated window, mean peak widths, SD, and RSD% were calculated (Tables S5 and S6).

2.7.3 | Definition of the Standardized Elution Window and Effective Pc Estimation

To enable a fair and unbiased comparison between HPDS and LPDS chromatographic performance, a standardized elution window (ΔCV_{global}) was defined based on HPDS separations. This window extended from the mean onset of Peak 8 (1.16 CV) to the mean end of Peak 1 (22.91 CV) (Table S6), yielding a total effective elution window of $\Delta CV_{global} = 21.75$ CV (Table 4).

The effective Pc was estimated according to the following relation:

$$P_c = 1 + \frac{\Delta CV_{global}}{\bar{w}} \quad (3)$$

where $\bar{w}$ corresponds to the mean peak base width calculated over all peaks eluting within the standardized window. This criterion was applied identically to both HPDS and LPDS systems.

2.7.4 | Pairwise Chromatographic Resolution (Rs) and Elution Distance ($\Delta CV_{pairwise}$) Determination

Local chromatographic resolution was quantitatively assessed using pairwise resolution factors (Rs) and elution distances ($\Delta CV_{pairwise}$) calculated between adjacent chromatographic peaks.

For each pair of consecutively eluting peaks, the resolution factor (Rs) was calculated in CV units according to the following

equation:

$$\mathbf{R_s} = \frac{2 \times \left(\mathbf{CV_{apex,2}} - \mathbf{CV_{apex,1}}\right)}{\boldsymbol{w}_1 + \boldsymbol{w}_2} \quad (4)$$

where $CV_{apex,1}$ and $CV_{apex,2}$ correspond to the apex positions of two adjacent chromatographic peaks, and w_1 and w_2 represent their respective peak base widths expressed in CV units. Peak apex positions and base widths were extracted from ELSD chromatograms using the same local baseline return criterion described above.

In addition to Rs, the elution distance between adjacent peaks was expressed as:

$$\boldsymbol{\Delta CV}_{\text{pairwise}} = \mathbf{CV_{apex,2}} - \mathbf{CV_{apex,1}} \quad (5)$$

Pairwise Rs and $\Delta CV_{pairwise}$ values were calculated for all adjacent UHM compounds under HPDS conditions and, where applicable, under LPDS conditions for peaks eluting within the standardized elution window. These metrics were used to quantitatively assess local chromatographic resolution and to complement the global Pc evaluation.

3 | Results and Discussion

3.1 | Evaluation of Scalability: From HPTLC to Flash Chromatography

The adaptation of the CDS method from HPTLC to normal-phase flash chromatography was initially assessed using the UHM as an SST. Figures 3 and 4 provide a direct qualitative comparison between HPTLC migration patterns and flash chromatographic elution profiles obtained under HPDS and LPDS conditions, respectively.

Concurrent analysis of the chromatographic profiles revealed a strong correspondence between the spots observed on HPTLC plates and the peaks detected by flash chromatography. Under both solvent systems, the least retained compound on HPTLC (Spot 8) systematically coincided with the first eluting peak in flash chromatography, while subsequent compounds (Spots 7 to 1) eluted sequentially according to increasing solvent strength. This conserved elution order demonstrates that retention behavior observed at the analytical HPTLC scale is preserved during transposition to preparative flash chromatography. This correlation is fully consistent with the polarity of the UHM compounds, as reflected by their Log *p* values (Table 1). Similar retention trends have been reported by Do et al. for CDS-based HPTLC analyses, supporting the robustness of polarity-driven separation across chromatographic scales [10].

For qualitative comparison purposes, the effective observation window extended from the start of the gradient to approximately 40 CV under both HPDS and LPDS conditions (Figures 3 and 4). Beyond this region, the final isocratic step at 100% of the most polar solvent of the system (methanol for HPDS, ethyl acetate for LPDS) primarily functioned as a rinsing phase to ensure complete elution of all analytes. While this extended window is relevant for visual comparison between HPTLC and flash chromatography, all quantitative chromatographic descriptors were intentionally calculated over a standardized elution window to ensure unbiased system comparison, as detailed below.

3.2 | Analysis of Retention Stability and Peak Width Characteristics

To ensure consistency across all quantitative descriptors, a standardized elution window was defined based on HPDS separations, spanning from the mean onset of Peak 8 (1.16 CV) to the mean end of Peak 1 (22.91 CV). This standardized window (ΔCV_{global} = 21.75 CV) was subsequently applied to both HPDS and LPDS systems for the calculation of peak base widths, pairwise resolution metrics, and effective Pc.

The intermediate precision of chromatographic retention, evaluated via the repeatability of CV_{apex} values, showed low RSDs for both solvent systems (generally < 5%), confirming high retention stability across independent runs (Table S5).

Peak base width determination showed good intermediate precision under both HPDS and LPDS conditions (Tables S6 and S7).

3.2.1 | HPDS System

Under HPDS conditions, peak base widths were narrow and highly reproducible across runs (Table 2). Early- and mid-eluting compounds within the standardized elution window exhibited mean base widths ranging from 0.60 to 0.9 CV for Peaks 8–7 and from 0.6 to 0.72 CV for Peaks 5–4. Broader peaks were observed only at higher CVs, with mean widths of 2.1–2.5 CV for Peaks 2–1. RSDs were generally below 15% (Table S6), confirming good intermediate precision and homogeneous chromatographic behavior across the elution window.

3.2.2 | LPDS System

In contrast, LPDS conditions induced systematic peak broadening, particularly for intermediate-eluting compounds (Table 2). Mean base widths increased from 1.8 CV (HPDS) to 3.4 CV (LPDS) for Peak 6 and from 0.6 CV (HPDS) to 2.4 CV (LPDS) for Peak 5. This broadening reflects an increased polarity-driven selectivity of the solvent system rather than a loss of chromatographic control, as the system maintains a consistent elution profile and provides a targeted redistribution of selectivity.

3.3 | Assessment of Local Separation Efficiency and Polarity-Driven Selectivity Redistribution

To complement global descriptors, local separation efficiency was evaluated using pairwise elution distance ($\Delta CV_{pairwise}$) and resolution factors (Rs) between adjacent peaks (Table 3). Under HPDS conditions, $\Delta CV_{pairwise}$ values remained relatively uniform, resulting in Rs values generally exceeding unity for most peak pairs. This reflects a balanced distribution of chromatographic resolution along the gradient.

TABLE 2 | Summary of peak base widths determined using a local baseline return criterion under HPDS and LPDS conditions.

Peak	HPDS — mean CV_{apex} (CV)	HPDS — mean width ± SD (CV)	LPDS — mean width ± SD (CV)*
8	1.384	0.60 ± 0.03	0.8 ± 0.3
7	3.5	0.9 ± 0.1	1.2 ± 0.3
6	6.4	1.8 ± 0.3	3.4 ± 0.6
5	12.74	0.6 ± 0.1	2.4 ± 0.3
4	13.28	0.72 ± 0.08	—
3	15.9	1.4 ± 0.1	—
2	18.92	2.1 ± 0.1	—
1	21.22	2.5 ± 0.2	—

Note: Values are reported as mean ± SD calculated from independent runs. The CV values reported correspond to mean CV_{apex} positions determined under HPDS conditions only (Table S5).

*LPDS values reported only for peaks eluting within the standardized window (1.16–22.91 CV). Under LPDS conditions, Compounds 4 and 3 eluted during the final column wash (Step 7) beyond this window and were therefore excluded from the width-based calculations used for Pc and local metrics.

TABLE 3 | Pairwise elution distance ($\Delta CV_{pairwise}$ and chromatographic resolution [Rs] between adjacent UHM compounds for HPDS and LPDS systems.

Peak pair	$\Delta CV_{pairwise}$ (HPDS)	Rs (HPDS)	$\Delta CV_{pairwise}$ (LPDS)	Rs (LPDS)
8–7	2.12	2.84	1.80	1.92
7–6	2.90	2.21	10.00	4.76
6–5	6.34	4.43	6.00	2.27
5–4	0.54	0.80	—	—
4–3	2.62	2.03	—	—
3–2	3.02	1.92	—	—
2–1	2.30	0.97	—	—

Note: $\Delta CV_{pairwise}$ was calculated according to Equation (5) and corresponds to the difference between the mean apex positions of two adjacent peaks. Rs was calculated according to Equation (4) using mean peak base widths determined from ELSD chromatograms. LPDS values are reported only for peak pairs eluting within the standardized elution window (1.16–22.91 CV).

TABLE 4 | Definition of the standardized elution window (ΔCV_{global}) used for effective Pc estimation.

Parameter	Value (CV)
Mean CV_{start} (Peak 8)	1.16
Mean CV_{end} (Peak 1)	22.91
ΔCV_{global}	21.75

Note: The window was defined from the mean onset of Peak 8 to the mean end of Peak 1 across all HPDS runs and was applied identically to HPDS and LPDS to enable a fair comparison.

Under LPDS conditions, $\Delta CV_{pairwise}$ and Rs values were reduced for selected adjacent peak pairs, most notably for Peaks 8–7 and 6–5 (Table 3), while remaining well above unity. Rather than indicating a loss of separation efficiency, these variations reflect a polarity-driven rescaling of the chromatographic elution space along the CV axis, whereby certain regions are expanded (e.g., Peaks 7–6) and others moderately contracted. This behavior results in a deliberate redistribution of chromatographic selectivity within the low-polarity domain, consistent with the complementary separation profiles observed in Figures 3 and 4.

3.4 | Global Performance Benchmarking via Effective Pc

To enable a fair and direct comparison between the HPDS and LPDS solvent systems, an effective Pc was calculated. Crucially, Pc was estimated over a standardized elution window (ΔCV_{global}) defined by the mean boundaries of the UHM elution under HPDS conditions, as detailed in Table 4.

As summarized in Table 5, HPDS yielded a higher effective peak capacity (Pc = 16.41), reflecting the narrow and homogeneous peak shapes observed across the gradient. In contrast, LPDS exhibited a lower Pc (Pc = 11.08), primarily due to the systematic increase in peak base widths for intermediate-eluting compounds. Within the CDS framework, this reduction in Pc is not interpreted as inferior performance, but rather as a deliberate shift toward enhanced polarity-dependent selectivity. Pc serves here as a system-dependent descriptor that, when

TABLE 5 | Effective Pc calculated over the standardized elution window.

Solvent system	Peaks included	Mean peak base width, ($\bar{w}$) (CV)	ΔCV_{global}	Pc
HPDS	8–1	1.326	21.75	16.41
LPDS	8–5	1.963	21.75	11.08

Note: Effective Pc calculated for HPDS and LPDS systems over the standardized elution window (ΔCV_{global} = 21.75 CV). Pc was estimated according to Equation 3.

considered alongside local resolution metrics (Rs), captures the complementary nature of the two solvent systems.

3.5 | Physicochemical Rationale for Step-Based Fractionation

The structured isocratic step-based fraction collection strategy is directly grounded in the quantitative chromatographic descriptors established in the previous sections. Rather than an arbitrary simplification, it represents a rational translation of polarity-driven behavior into a standardized fractionation scheme.

As established by the conserved elution order between HPTLC and flash chromatography (Figures 3 and 4), compound retention is primarily governed by polarity, a trend closely mirrored by the calculated Log *p* values of the UHM compounds (Table 1). The relevance of this approach is confirmed by the co-migration of selected UHM fractions on HPTLC (Figure 3B). Specifically, Compound 2 is present in HPDS fraction F3 but absent from LPDS fraction F7, indicating that the latter effectively subdivides the third HPDS isocratic step. This observation is mathematically supported by the experimental retention data: Compound 3 concludes its elution at a mean CV_{end} of 16.82 CV, while the subsequent peak (Compound 2) starts eluting at 18.29 CV (Table S6). Consequently, the LPDS fractionation window (F1–F7) covers the 0 to ~16 CV region of the HPDS chromatogram, as precisely marked by the 16 CV tick mark in Figure 3A.

Reciprocal experiments (Figure 4B) further reinforce this interpretation, as HPDS fractions F1–F3 are shown to encompass the entire set of compounds observed across all seven LPDS fractions. This confirms that LPDS does not explore an orthogonal chemical space but operates as a "polarity-focused magnification" of the low-polarity domain sampled more broadly under HPDS conditions.

3.6 | Application to a Complex Matrix and Benefits for Downstream Metabolomic Workflows

The applicability and robustness of the flash–CDS strategy were further evaluated using a crude methanolic extract of *S. scardica*. Flash fractionation followed by HPTLC analysis confirmed that the so-called "polarity zoom" effect and the fractionation boundaries remain consistent even in a highly complex non-model matrix (Figures 5 and 6).

Under HPDS conditions (Figure 5B), LPDS fraction F7 excludes constituents present in HPDS fraction F3 with Rf values between 0.4 and 0.9, while retaining those migrating at very high Rf (0.9–1.0). This HPTLC pattern is perfectly synchronized with the flash chromatogram (Figure 5A), where a discrete signal terminates at ~16 CV (corresponding to the high Rf spots), while more polar compounds (Rf 0.4–0.9) only begin to elute around 17 CV. This confirms that the transition at ~16 CV is a reproducible cutoff for subdividing the extract's metabolome.

Beyond polarity mapping, this systematic fractionation strategy offers several practical advantages for untargeted workflows:

i. *Detector independence*: By decoupling collection from detector thresholds, the method ensures the capture of analytes lacking strong chromophores or present at trace levels. This is clearly demonstrated by fractions HPDS F5 (UHM) and HPDS F7 (extract), which contain distinct HPTLC spots despite near-baseline UV/ELSD signals.

ii. *Handling unresolved profiles*: For complex profiles like those observed under LPDS (Figure 6A), where distinct chromatographic peaks are absent, systematic collection ensures that no chemical information is lost due to detector insensitivity or peak coalescence.

iii. *Mitigation of matrix effects*: The reduction of chemical complexity within individual fractions is expected to significantly reduce ion suppression during subsequent LC-HRMS/MS analysis, a critical factor for improving the quality of metabolic annotation.

iv. *Standardized coordinate system*: Fixed boundaries allow for superior data alignment across different samples, as equivalent fractions correspond to comparable polarity ranges. While the inherent partial overlap between adjacent fractions may be seen as a drawback, this redundancy provides multiple analytical "views" of the same analyte, which can serve to cross-validate molecular features during future dereplication efforts.

Overall, these results demonstrate that the flash–CDS strategy provides a robust and chemically meaningful pre-fractionation platform under the conditions investigated, particularly for polarity-driven extract simplification. By streamlining the transition from crude extracts to simplified, polarity-defined fractions, it constitutes a valuable bridge toward high-confidence metabolomic characterization.

3.7 | Integration of Flash–CDS Into the Natural Products Discovery Pipeline

The flash–CDS strategy is proposed as a modular component in modern metabolomics and drug discovery workflows. By system-

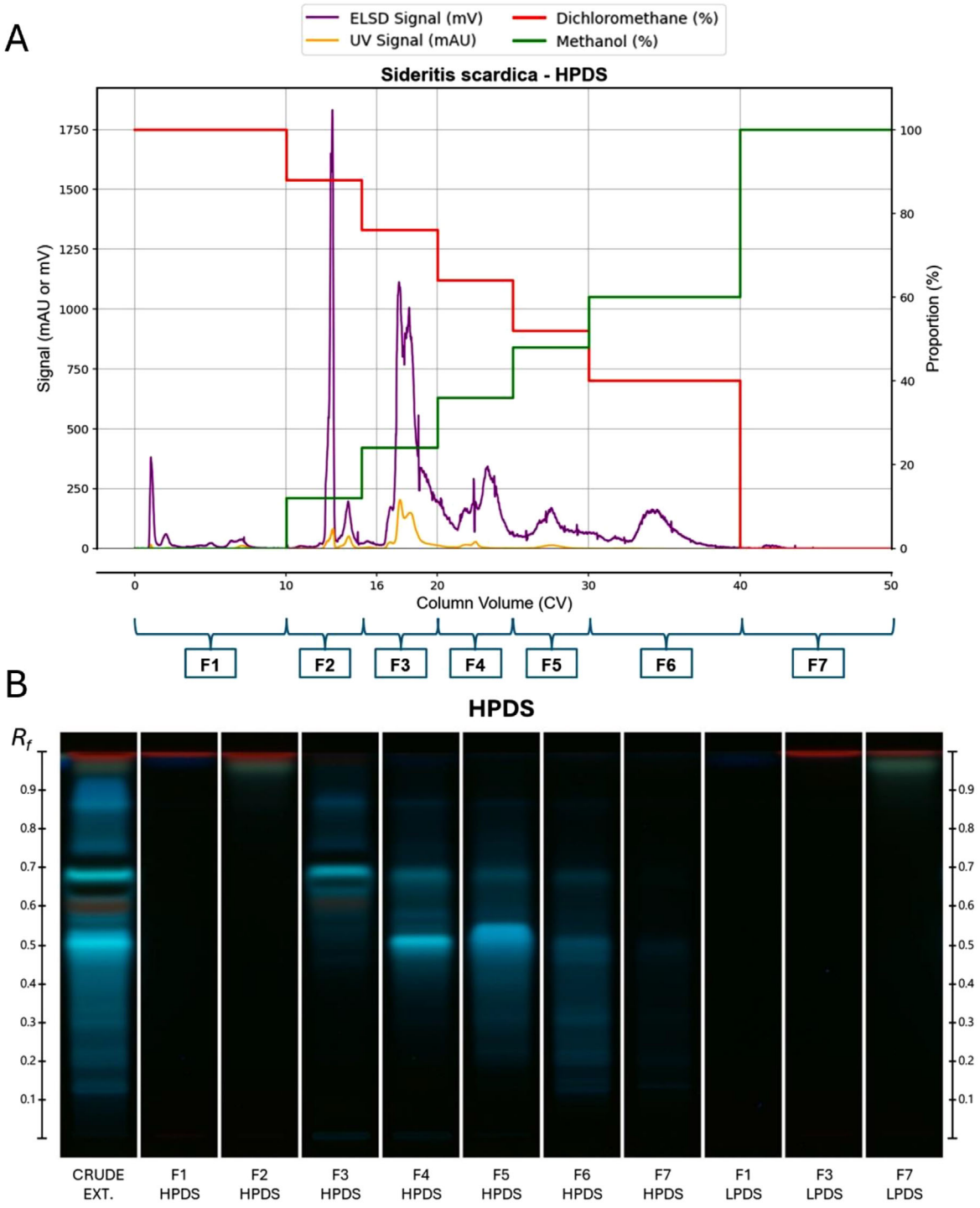

FIGURE 5 | Comparative analysis of flash chromatography and HPTLC separation of a crude methanolic extract of *Sideritis scardica* under HPDS conditions. (A) Flash chromatogram obtained using the adapted HPDS solvent system in normal-phase flash chromatography. The ELSD signal (purple) and UV signal (orange) are displayed as a function of CV and overlaid with the stepwise solvent gradient expressed as proportions of dichloromethane (red) and methanol (green). λ (UV): 250–600 nm. The predefined isocratic steps corresponding to fractions F1–F7 collected under HPDS conditions are indicated below the chromatogram. A tick mark at 16 CV highlights the boundary corresponding to the LPDS fractionation window. (B) HPTLC plate developed using the HPDS solvent system. Lanes include the crude methanolic extract of *S. scardica*, HPDS flash fractions F1–F7, and selected fractions obtained under LPDS conditions (F1 LPDS, F3 LPDS, and F7 LPDS). Plate was derivatized using Neu/PEG reagent and visualized at 366 nm. This panel enables direct comparison between HPDS and LPDS fractionation domains for a complex botanical extract and illustrates the distribution of compounds across polarity-defined fractions.

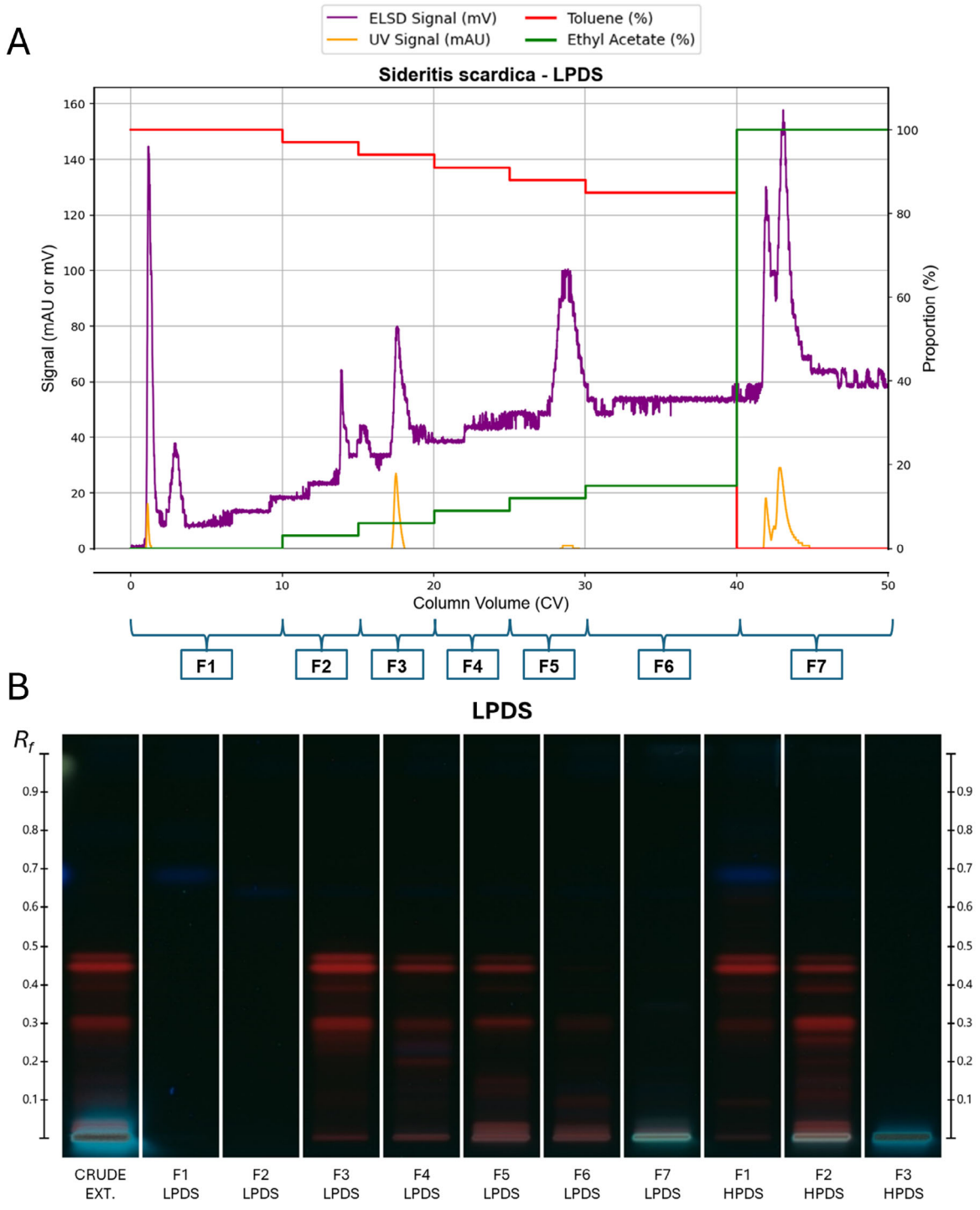

FIGURE 6 | Comparative analysis of flash chromatography and HPTLC separation of a crude methanolic extract of *Sideritis scardica* under LPDS conditions. (A) Flash chromatogram obtained using the adapted LPDS solvent system in normal-phase flash chromatography, plotted as a function of CV. The ELSD signal (purple) and UV signal (orange) are superimposed with the stepwise solvent gradient expressed as proportions of toluene (red) and ethyl acetate (green). λ (UV): 290–800 nm. The predefined isocratic steps corresponding to fractions F1–F7 collected under LPDS conditions are indicated below the chromatogram. (B) HPTLC plate developed using the LPDS solvent system. Lanes include the crude methanolic extract of *S. scardica*, LPDS flash fractions F1–F7, and selected fractions obtained under HPDS conditions (F1 HPDS, F2 HPDS, and F3 HPDS). Plate was derivatized using Neu/PEG reagent and visualized at 366 nm. This panel allows visualization of the chemical space covered by LPDS fractions relative to HPDS-derived fractions and illustrates the complementary polarity selectivity of both solvent systems when applied to a complex botanical matrix.

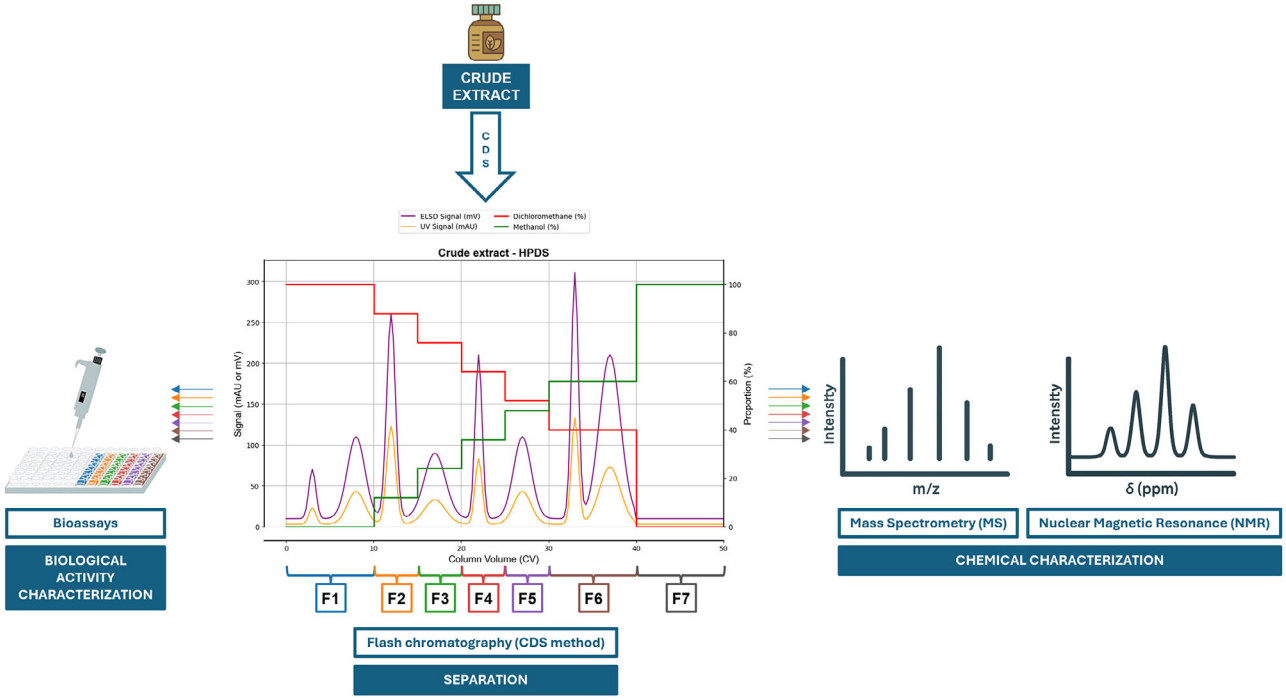

FIGURE 7 | Integrated workflow for the application of the flash–CDS strategy into natural product discovery. The crude extract is fractionated via flash chromatography using the CDS method, where each isocratic step (F1–F7) corresponds to a predefined polarity-defined window. This structured collection is intended to enable parallel downstream processing: (i) biological screening for activity characterization and (ii) chemical profiling via MS and/or NMR. The scheme illustrates a representative HPDS-based separation and highlights the demonstrated transition from complex mixtures to simplified, polarity-defined fractions suitable for downstream analyses.

atically simplifying crude extracts into polarity-defined fractions, this method directly addresses the persistent challenge of chemical complexity that often hinders high-throughput screening and metabolic profiling [35]. As illustrated in the integrated workflow (Figure 7), the standardized, polarity-defined nature of the fractions suitable for a dual-track evaluation: biological activity can be mapped directly onto the polarity-gradient while chemical characterization (MS/NMR) is performed on significantly less complex matrices.

This approach bridges the gap between the speed of non-targeted analysis and the high resolution of classical isolation, aligning with modern strategies in natural product research that prioritize early extract simplification to enhance dereplication efficiency [36].

The benefits of such pre-fractionation strategies are well-documented in the literature. For instance, Olivon et al. demonstrated that systematic flash chromatography fractionation coupled with molecular networking enabled the guided isolation of both known and novel diterpenes [37]. Similarly, large-scale natural extract libraries, such as those established by Wyeth using HPLC pre-fractionation, have proven that reducing mixture complexity significantly improves biological screening yields and accelerates the characterization of active hits [38].

Compared to these established methods, the flash–CDS approach offers several tangible advantages within a polarity-driven, flash-based fractionation framework:

i. *Rationalization and exhaustiveness*: By providing a standardized coordinate system based on universal polarity markers (UHM), the method ensures a more reproducible fractionation than peak-based collection.

ii. *Computational synergy*: The standardization of the process facilitates the comparison of chemical profiles across different extracts, allowing for the potential compilation of chromatographic and spectrometric data into databases for advanced computational processing.

iii. *Efficiency*: The reduction in the number of fractions (limited to seven per system) while maintaining high chemical coverage significantly reduces the analytical burden on downstream LC-HRMS/MS and NMR platforms.

In conclusion, the integration of flash–CDS into analytical pipelines—synergizing with advancements in detection techniques and modern bioinformatics tools—has the potential to accelerate the discovery of bioactive principles. By minimizing the need for laborious, repetitive isolation steps, this methodology provides a robust experimental foundation for high-confidence dereplication and the discovery of novel substances in polarity-oriented natural product workflows.

4 | Conclusion

In this study, the CDS method was successfully transposed from HPTLC to normal-phase flash chromatography, providing a ratio-

nal and reproducible proof-of-concept framework for polarity-driven fractionation. Using the UHM as an SST, we demonstrated that chromatographic retention behavior is robustly conserved across scales, as evidenced by the strong correspondence between HPTLC migration (Rf) and flash elution volumes (CV).

Quantitative evaluation of peak dispersion, local resolution, and effective Pc highlighted the complementary nature of the two solvent systems. While HPDS provided a globally balanced separation characterized by narrow and homogeneous peak distributions, LPDS deliberately redistributed chromatographic selectivity toward the low-polarity domain, acting as a polarity-focused magnification tool rather than an orthogonal separation mode. Importantly, these solvent-dependent behaviors were not limited to a reference mixture but were reproducibly observed when applied to a chemically complex methanolic extract of *S. scardica* Griseb., supporting the applicability of the CDS framework to botanical matrices under the conditions investigated.

Beyond chromatographic performance, the structured isocratic step-based fractionation strategy provides several practical advantages for untargeted workflows. By decoupling fraction collection from detector-based thresholds, the method facilitates the recovery of chemical constituents, including compounds present at low abundance or lacking strong chromophores. The resulting polarity-defined fractions reduce sample complexity and establish a consistent polarity-based coordinate system, which is particularly advantageous for downstream LC-HRMS/MS analysis, dereplication, and data alignment across samples.

Overall, the flash–CDS strategy illustrates how flash chromatography can be rationally adapted into a chemically meaningful pre-fractionation platform. By bridging analytical-scale screening and downstream structural characterization, this proof-of-concept approach demonstrates strong potential for integration into modern natural product workflows. Future work will focus on extending this strategy to additional plant matrices and biological applications to further assess its robustness, scalability, and general applicability.

Author Contributions

Jason Fauquet: conceptualization, investigation, visualization, methodology, data curation, formal analysis, writing – original draft, writing – original draft preparation. **Adam Ellatiff**: investigation, writing – review and editing. **Claudio Palmieri**: conceptualization, investigation, writing – review and editing. **Mathilde Wells**: supervision, writing – review and editing. **Pierre Duez**: supervision, writing – review and editing. **Bertr**and **Blankert**: supervision, writing – review and editing. **Amandine Nachtergael**: conceptualization, funding acquisition, supervision, resource, writing – review and editing

Acknowledgments

We express our sincere gratitude to Prof. R. Wattiez from the Proteomics and Microbiology (ProtMic) Unit for granting us access to the UMONS Bioprofiling Platform. The Bioprofiling platform used for proteomic analysis was supported by the European Regional Development Fund and the Walloon Region, Belgium.

Conflicts of Interest

The authors declare no conflicts of interest.

Data Availability Statement

The authors confirm that the data supporting the findings of this study are available within the article [and/or] its Supporting Information.

References

1. M. Zych and A. Pyka-Pająk, "TLC in the Analysis of Plant Material," *Processes* 13 (2025): 3497.

2. T. K. T. Do, M. Schmid, I. Trettin, M. Hänni, and E. Reich, "Complementary Developing Solvents for Simpler and More Powerful Routine Analysis by High-Performance Thin-Layer Chromatography," *Journal of Planar Chromatography - Modern TLC* 35 (2022): 299–311, https://doi.org/10.1007/s00764-022-00185-1.

3. T. Brendler, *African Herbal Pharmacopoeia* (Association for African Medicinal Plants Standards, 2010).

4. T. K. T. Do and E. Reich, "Insights Into the Evolution and Future of High-Performance Thin-Layer Chromatography in Routine Quality Control: A Review," *Journal of Planar Chromatography - Modern TLC* 36 (2023): 317–325, https://doi.org/10.1007/s00764-023-00265-w.

5. "Polarity Index," Louisana State University, accessed February 11, 2025, https://macro.lsu.edu/howto/solvents/Polarity%20index.htm.

6. L. R. Snyder, "Classification off the Solvent Properties of Common Liquids," *Journal of Chromatographic Science* 16 (1978): 223–234, https://doi.org/10.1093/chromsci/16.6.223.

7. L. R. Snyder, "Classification of the Solvent Properties of Common Liquids," *Journal of Chromatography A* 92 (1974): 223–230, https://doi.org/10.1016/S0021-9673(00)85732-5.

8. A. Kumar, A. Pandey, N. K. Gaur, et al., "Development and Validation of HPTLC Fingerprint Method for 16 Homeopathic Mother Tinctures Lacking Standards," *Biomedical Chromatography* 39 (2025): e70194, https://doi.org/10.1002/bmc.70194.

9. S. N. Meyyanathan, P. Kumar, and B. Suresh, "Analysis of Tramadol in Pharmaceutical Preparations by High Performance Thin Layer Chromatography," *Journal of Separation Science* 26 (2003): 1359–1362, https://doi.org/10.1002/jssc.200301541.

10. T. K. T. Do, M. Schmid, M. Phanse, et al., "Development of the First Universal Mixture for Use in System Suitability Tests for High-Performance Thin Layer Chromatography," *Journal of Chromatography A* 1638 (2021): 461830, https://doi.org/10.1016/j.chroma.2020.461830.

11. E. Reich and A. Schibli, *High-Performance Thin-Layer Chromatography for the Analysis of Medicinal Plants* (Thieme, 2007).

12. K. Schuster and C. Oellig, "Effect of Relative Humidity on the Thin-Layer Chromatographic Separation of E 472 Emulsifiers," *Journal of Planar Chromatography – Modern TLC* 36 (2023): 327–334.

13. A. Ammar, "Analysis of Drug Substances by Using New Concepts of HPLC and Development of Some HPTLC Methods," (PhD diss., 2009, Freien Universität Berlin).

14. M. Schmid, T. K. T. Do, I. Trettin, and E. Reich, "Applicability of the Universal Mixture for Describing System Suitability and Quality of Analytical Data in Routine Normal Phase High Performance Thin Layer Chromatography Methods," *Journal of Chromatography A* 1666 (2022): 462863, https://doi.org/10.1016/j.chroma.2022.462863.

15. A. Balkrishna, P. Sharma, M. Joshi, J. Srivastava, and A. Varshney, "Development and Validation of a Rapid High-Performance Thin-Layer Chromatographic Method for Quantification of Gallic Acid, Cinnamic Acid, Piperine, Eugenol, and Glycyrrhizin in Divya-Swasari-Vati, an Ayurvedic Medicine for Respiratory Ailments," *Journal of Separation Science* 44 (2021): 3146–3157, https://doi.org/10.1002/jssc.202100096.

16. Y.-P. Zhang, S.-Y. Shi, X. Xiong, X.-Q. Chen, and M.-J. Peng, "Comparative Evaluation of Three Methods Based on High-Performance Liquid Chromatography Analysis Combined with a 2,2′-Diphenyl-1-Picrylhydrazyl Assay for the Rapid Screening of Antioxidants From *Pueraria lobata* Flowers," *Analytical and Bioanalytical Chemistry* 402 (2012): 2965–2976, https://doi.org/10.1007/s00216-012-5722-3.

17. M. Walasek-Janusz, K. K. Wojtanowski, R. Papliński, A. Grzegorczyk, and R. Nurzyńska-Wierdak, "Polyphenol Profile and Biological Activity of the Extracts From *Sideritis scardica* Griseb. (Lamiaceae) Herb," *Pharmaceuticals* 18 (2025): 1121, https://doi.org/10.3390/ph18081121.

18. B. Janeska, M. Stefova, and K. Alipieva, "Assay of Flavonoid Aglycones From the Species of Genus *Sideritis* (Lamiaceae) From Macedonia With HPLC-UV DAD," *Acta Pharmaceutica* 57 (2007): 371–377.

19. V. Tadić, D. Bojović, I. Arsić, et al., "Chemical and Antimicrobial Evaluation of Supercritical and Conventional *Sideritis scardica* Griseb., Lamiaceae Extracts," *Molecules* 17 (2012): 2683–2703.

20. M. Todorova and A. Trendafilova, "*Sideritis scardica* Griseb., an Endemic Species of Balkan Peninsula: Traditional Uses, Cultivation, Chemical Composition, Biological Activity," *Journal of Ethnopharmacology* 152 (2014): 256–265, https://doi.org/10.1016/j.jep.2014.01.022.

21. C. Knox, M. Wilson, C. M. Klinger, et al., "DrugBank 6.0: The DrugBank Knowledgebase for 2024," *Nucleic Acids Research* 52 (2024): D1265–D1275, https://doi.org/10.1093/nar/gkad976.

22. "What is PubChem?" PubChem, accessed February 12, 2025, https://pubchem.ncbi.nlm.nih.gov/.

23. "Search," CAS SciFinder, accessed February 12, 2025, https://scifinder-n.cas.org/?referrer=scifinder.cas.org.

24. V. Taco, "Eco-Friendly Extraction of Bioactive Metabolites From Ecuadorian Quinoa (Chenopodium quinoa Willd.) by Natural Deep Eutectic Solvents (NADES)," Doctoral dissertation, University of Mons, Mons, Belgium, 2022.

25. European Pharmacopoeia, General chapter 2.8.25, European Pharmacopeoia, 11th ed., Council of Europe, Strasbourg, 2025.

26. United States Pharmacopeia, General Chapter ⟨203⟩ High-Performance Thin-Layer Chromatography Procedure for Identification of Articles of Botanical Origin. USP-NF. United States Pharmacopeia, Rockville, MD 2019, https://doi.org/10.31003/USPNF_M9134_02_01.

27. Interchim, "Ultra Performance Flash Purification: Or How to Do High Throughput Purification, G6," 2020, https://www.advion.com/rsc-brochure/ultra-performance-flash-purification-how-to-do-high-throughput-purification/.

28. Interchim, Ultra Performance Flash Purification: Or How to Do High Throughput Purification, B19. 2020, https://www.advion.com/rsc-brochure/ultra-performance-flash-purification-how-to-do-high-throughput-purification/.

29. L. R. Snyder, J. J. Kirkland, and J. W. Dolan, *Introduction to Modern Liquid Chromatography* (John Wiley & Sons, 2009), 361–402, https://doi.org/10.1002/9780470508183.

30. R. P. W. Scott, "The Silica-Gel Surface and Its Interactions With Solvent and Solute in Liquid Chromatography," *Faraday Symposia of the Chemical Society* 15 (1980): 49, https://doi.org/10.1039/fs9801500049.

31. R. J. Capon, "Extracting Value: Mechanistic Insights Into the Formation of Natural Product Artifacts—Case Studies in Marine Natural Products," *Natural Product Reports* 37 (2020): 55–79, https://doi.org/10.1039/C9NP00013E.

32. J. R. Hanson, "Pseudo-Natural Products, Some Artefacts Formed During the Isolation of Terpenoids," *Journal of Chemical Research* 41 (2017): 497–503, https://doi.org/10.3184/174751917X15021050367558.

33. L. R. Snyder, J. J. Kirkland, and J. W. Dolan, *Introduction to Modern Liquid Chromatography* (John Wiley & Sons, 2009), 199–252, https://doi.org/10.1002/9780470508183.

34. S. Nyiredy, "Planar Chromatographic Method Development Using the PRISMA Optimization System and Flow Charts," *Journal of Chromatographic Science* 40 (2002): 553–563, https://doi.org/10.1093/chromsci/40.10.553.

35. J. D. Santos, I. Vitorino, F. Reyes, F. Vicente, and O. M. Lage, "From Ocean to Medicine: Pharmaceutical Applications of Metabolites From Marine Bacteria," *Antibiotics* 9 (2020): 455, https://doi.org/10.3390/antibiotics9080455.

36. J.-L. Wolfender, M. Litaudon, D. Touboul, and E. Ferreira Queiroz, "Innovative Omics-Based Approaches for Prioritisation and Targeted Isolation of Natural Products—New Strategies for Drug Discovery," *Natural Product Reports* 36 (2019): 855–868, https://doi.org/10.1039/C9NP00004F.

37. F. Olivon, P.-M. Allard, A. Koval, et al., "Bioactive Natural Products Prioritization Using Massive Multi-Informational Molecular Networks," *ACS Chemical Biology* 12 (2017): 2644–2651, https://doi.org/10.1021/acschembio.7b00413.

38. M. M. Wagenaar, "Pre-Fractionated Microbial Samples—The Second Generation Natural Products Library at Wyeth," *Molecules* 13 (2008): 1406–1426, https://doi.org/10.3390/molecules13061406.

Supporting Information

Additional supporting information can be found online in the Supporting Information section.

Supporting File 1: jssc70376-sup-0001-FigureS1.tif.
Supporting File 2: jssc70376-sup-0002-FigureS2.tif.
Supporting File 3: jssc70376-sup-0003-FigureS3.tif.
Supporting File 4: jssc70376-sup-0004-TableS1.docx.
Supporting File 5: jssc70376-sup-0005-TableS2.docx.
Supporting File 6: jssc70376-sup-0006-TableS3.docx.
Supporting File 7: jssc70376-sup-0007-TableS4.docx.
Supporting File 8: jssc70376-sup-0008-TableS5.docx.
Supporting File 9: jssc70376-sup-0009-TableS6.docx.
Supporting File 10: jssc70376-sup-0010-TableS7.docx.
Supporting File 11: jssc70376-sup-0011-TableS8.docx.
Supporting File 12: jssc70376-sup-0012-SuppMat.DOCX.